Journal of
Applied Crystallography
ISSN 0021-8898

Received 3 October 2011
Accepted 9 January 2012

Grazing-incidence in-plane X-ray diffraction on ultra-thin organic films using standard laboratory equipment

Markus Neuschitzer,[a]* Armin Moser,[a] Alfred Neuhold,[a] Johanna Kraxner,[b] Barbara Stadlober,[b] Martin Oehzelt,[c] Ingo Salzmann,[d] Roland Resel[a] and Jiří Novák[a]

[a]Institute of Solid State Physics, Graz University of Technology, Austria, [b]Joanneum Research Forschungsgesellschaft mbH, Institute of Surface Technologies and Photonics, Weiz, Austria, [c]Helmholtz Zentrum Berlin für Materialien und Energie – BESSY II, Germany, and [d]Institut für Physik, Humbold Universität zu Berlin, Germany. Correspondence e-mail: n_markus@sbox.tugraz.at

A novel grazing-incidence in-plane X-ray diffraction setup based on a commercial four-circle diffractometer with a sealed-ceramic copper X-ray tube, upgraded with parabolic graded multilayer X-ray optics and a one-dimensional position-sensitive detector, is presented. The high potential of this setup is demonstrated by a phase analysis study of pentacene thin films and the determination of in-plane lattice constants of pentacene mono- and multilayers. The quality of the results compare well to studies performed at synchrotron radiation facilities.

1. Introduction

Grazing incidence in-plane X-ray diffraction (GIXD) is a powerful technique to solve problems in materials science. First established by Marra *et al.* (1979) to study crystal surfaces and interfaces, it is now widely used to determine in-plane order and crystalline properties of thin films. In GIXD, X-rays impinge on the sample surface at a grazing angle below the angle of total external reflection, resulting in an evanescent wave propagating parallel to the surface. Perpendicular to the surface, its amplitude is exponentially damped, *i.e.* its penetration depth is limited to several nanometres depending on the incidence angle, the wavelength of the radiation and the electron density of the material (Vineyard, 1982). Therefore, in a GIXD experiment the evanescent wave is scattered only by the first few surface layers, resulting in an exceedingly increased surface sensitivity. Moreover, the wavefield amplitude of the evanescent wave is enhanced up to a factor of two because incident, reflected and transmitted wavefields couple coherently at the surface (Dosch, 1992). As a result, GIXD allows scattering experiments to be performed on thin films of very low scattering volume (Resel *et al.*, 2006; Novák *et al.*, 2011). Because of its scattering geometry (see Fig. 1), GIXD probes lattice planes that are almost perpendicular to the surface, and thus the in-plane structure of the sample can be determined. GIXD even allowed, for the first time, the characterization of the structure of ordered organic monolayers (Als-Nielsen *et al.*, 1994; Kaganer *et al.*, 1999).

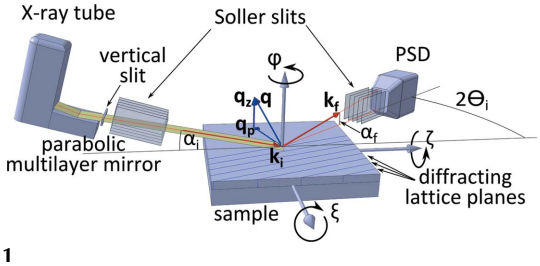

Figure 1
Schematic of the experimental setup. The wavevectors of the incident wave and a scattered wave ($\mathbf{k}_i$ and $\mathbf{k}_f$, respectively), the corresponding scattering vector $\mathbf{q}$, and its in-plane and out-of-plane components (q_p and q_z, respectively) as well as the probed lattice planes are indicated. A detailed description is given in the text.

Nowadays, GIXD measurements are mostly performed using synchrotron radiation sources of high brilliance. However, an increasing interest in GIXD setups in laboratories arose with the emergence of more sophisticated X-ray optics (Tanner *et al.*, 2004). This work shows in detail the realization of a novel GIXD setup in the laboratory and its successful application on pentacene thin films and monolayers. Even for monolayer films, we demonstrate that our setup allows us to achieve results comparable to those obtained by a synchrotron radiation facility.

2. Experimental setup

The GIXD setup is based on a commercial four-circle Bruker D8 Discover diffractometer upgraded with the Bruker Ultra GID add-on, which allows rotation of the X-ray tube to set the angle of incidence (α_i) of the X-ray beam towards the substrate surface. It is possible to tune the angle of incidence between −3.5 and 6.5° with a resolution better than 0.01° while keeping the sample horizontal; the experimental setup is illustrated in Fig. 1.

A conventional 2.2 kW water-cooled X-ray tube with a copper anode in line-focus mode is used as X-ray source. The divergent X-ray beam emitted from the line-shaped source is collimated by a 60 mm-long parabolic graded multilayer mirror (Schuster & Gobel, 1995), leading to an out-of-plane divergence better than 0.025°. In addition, the multilayer mirror acts as monochromator, which suppresses the intensity of Cu $K\beta$ radiation to less than 1% of the Cu $K\alpha$ radiation. The in-plane incoming beam divergence is adjusted by Soller slits to 0.35°. The resulting beam has dimensions of 1.1 mm in height and 12 mm in width and can be limited in height by a vertical slit after the multilayer mirror. The reached flux density of the X-ray beam is 8.6×10^6 photons $(\text{s mm}^2)^{-1}$.

The sample is attached to an Eulerian cradle with a sample stage that allows translations in all three directions (x, y, z) and rotations around the vertical axis (φ). In addition, the sample holder can be tilted in two perpendicular directions (ξ, ζ) to align the sample surface normal to the rotation axis (φ).

To reduce measurement time, a one-dimensional position-sensitive detector (PSD; Vantec-1; Khazins *et al.*, 2004) is used to collect scattering intensity profiles along the out-of-plane direction with a resolution of $\Delta\alpha_f = 0.007^\circ$. The angular resolution of the PSD is calibrated by scanning the X-ray angle of incidence (α_i) from the lowest to the highest possible value, *i.e.* by scanning the (attenuated) primary X-ray beam over the whole detector range. Thus a linear dependency between the detector read-out channels and the exit angle (α_f) can be calculated. In our present setup, the PSD covers an out-of-plane range (α_f) of 7.3° in one single shot. A set of Soller slits in front of the PSD defines the angular in-plane detector acceptance as 0.35°.

The presented scattering geometry probes lattice planes that are nearly perpendicular to the sample surface, as indicated in Fig. 1. Thus, this setup is perfectly suited to characterize the in-plane order of epitaxially grown films as well as two-dimensional powders (*i.e.* fiber-textured films). In such samples, all crystallites are oriented with the identical lattice plane parallel to the substrate surface while their azimuthal orientations (*i.e.* with respect to the sample surface) are statistically distributed. This specific growth mode is typically found for ordered organic monolayers or organic thin films grown on isotropic surfaces. In this case, complete crystallographic information can be revealed by in-plane diffraction at one specific azimuthal angle φ (Mannsfeld *et al.*, 2011; Salzmann *et al.*, 2011; Moser *et al.*, 2009).

3. Experimental details and data processing

The experimental results of the GIXD measurements are visualized and analyzed using the custom-made software *PyGid* (Moser, 2011), which allows transformation to q space, indexing of Bragg peaks, and intensity extraction into horizontal and vertical directions. In the following, GIXD data are shown as reciprocal-space maps (RSMs) as a function of the in-plane component q_p and out-of-plane component q_z of the scattering vector $\mathbf{q}$ [$q = (4\pi/\lambda)\sin\theta$] (Fig. 1). The intensities recorded with the one-dimensional PSD were corrected using a flat-field correction to guarantee equal sensitivity over the whole detector range. RSMs of all presented samples were measured under ambient conditions with an incidence angle equal to the critical angle of total external reflection of pentacene, which corresponds to 0.17° for Cu $K\alpha$ radiation ($\lambda_{Cu\,K\alpha} = 1.542$ Å). For the used vertical slit size of 0.6 mm, this incidence angle leads to a 202 mm footprint of the direct beam on the sample surface plane. The sample size of all investigated samples was 20 × 20 mm.

4. Experimental setup performance

4.1. Pentacene 50 nm thin films

Pentacene, one of the most thoroughly studied materials in the field of organic electronics, exhibits several polymorphs slightly different from its bulk crystal structure (Mattheus *et al.*, 2001). Pentacene deposited as a thin film on SiO_2 grows as a two-dimensional powder, making in-plane diffraction necessary to solve its crystal structure, as was shown independently by Yoshida *et al.* (2007), Nabok *et al.* (2007) and Schiefer *et al.* (2007). An RSM of a nominally 50 nm thin pentacene film prepared on a thermally oxidized silicon wafer (SiO_2) is depicted in Fig. 2(*a*). This RSM was recorded with a step size of $\Delta 2\theta_i = 0.05^\circ$ using the described setup (integration time of 180 s per step). The presence of a dominating thin-film-phase portion (black dots) and an additional less pronounced contribution of the bulk phase (white dots) (Campbell *et al.*, 1962) can clearly be seen.

A comparison between synchrotron and laboratory data is presented in Fig. 2(*b*). Synchrotron measurements were carried out at the HASYLAB (DESY, Hamburg, Germany) Doris W1 beamline using a wavelength $\lambda = 1.180$ Å, an incidence angle of $\alpha_i = 0.15^\circ$, a step size of $\Delta 2\theta_i = 0.05^\circ$ and an integration time of 2 s per step. For detection, a one-dimensional Mythen detector was employed, which covers an out-of-plane range (α_f) of 4° in one shot. In the used configuration the primary beam reaches a flux density of 3.1×10^{10} photons (s mm^2)$^{-1}$. The beamline provides a good trade-off between intensity and beam damage since beam damage plays a nonnegligible role in the characterization of organic materials using synchrotron radiation (Neuhold *et al.*, 2012). In Fig. 2(*b*) the diffraction intensities integrated over a q_z range from 0 to 0.46 Å^{-1} followed by background subtraction are shown for the same pentacene thin-film sample. Each peak was fitted with a Lorentzian to compare the peak areas and full widths at half-maximum (FWHMs).

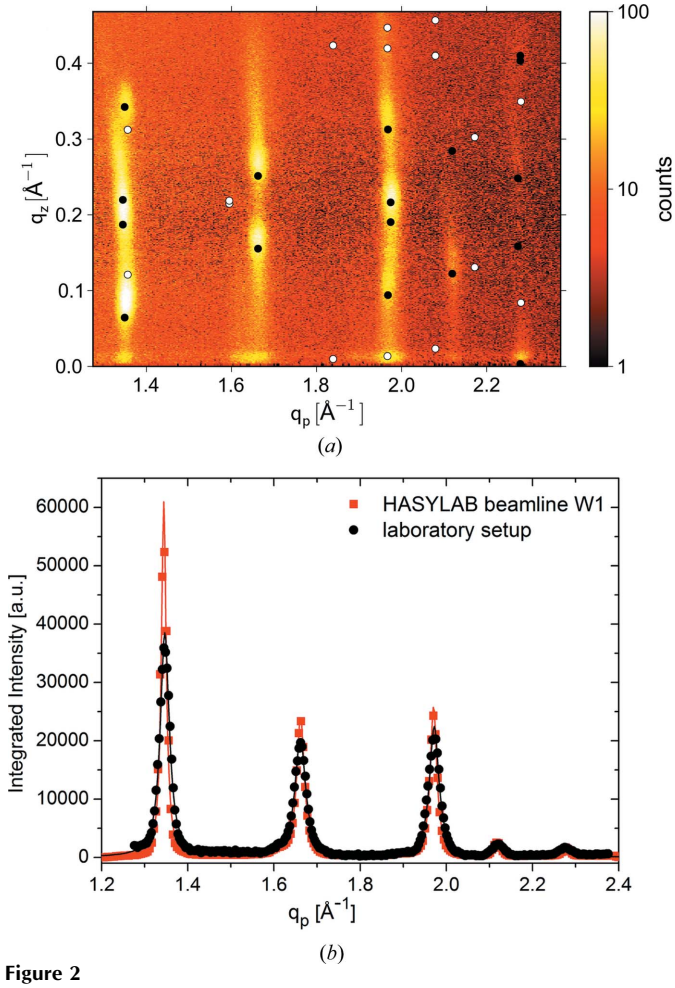

Figure 2
(*a*) Grazing-incidence reciprocal-space map of a 50 nm pentacene film grown on SiO_2 measured with the laboratory setup. Reflections corresponding to the pentacene thin-film phase are indicated with black dots, bulk-phase contributions with white dots. (*b*) Comparison between beamline W1 (HASYLAB) and the laboratory measurements (red squares and black dots, respectively). Intensities are integrated over a q_z range from 0 to 0.46 Å^{-1} and afterwards corrected for background. The peaks are fitted with Lorentzians (full lines).

The ratio found between the peak area measured in the laboratory and that measured at the synchrotron was 1.2. Hence, a 50 times longer total measurement time in the laboratory (16.5 h) than at the synchrotron (20 min) results in comparable quality. This is still a reasonable measurement time for normal laboratories. Comparing integrated count rates of the peaks reveals that a 100 times longer integration time is needed in the laboratory for statistics equivalent to the synchrotron measurement.

The peak widths (FWHM) of the synchrotron data are smaller than the peaks of the laboratory measurement, *e.g.* 0.014 Å^{-1} (HASYLAB) *versus* 0.024 Å^{-1} (laboratory) for the first, 0.021 *versus* 0.03 Å^{-1} for the second, and 0.018 *versus* 0.029 Å^{-1} for the third peak. This is due to a worse in-plane resolution in the laboratory. The in-plane resolution of the laboratory equipment is determined by the Soller slits. Their angular acceptance has to be chosen as a trade-off between intensity (*i.e.* measurement time necessary to obtain the requested measurement statistics) and resolution. The FWHM in reciprocal space of the first peak (0.024 Å^{-1}) corresponds to 0.34° in angular space, *i.e.* exactly the angular acceptance of the Soller slits (0.35°). The FWHMs of the second and third peaks are slightly larger

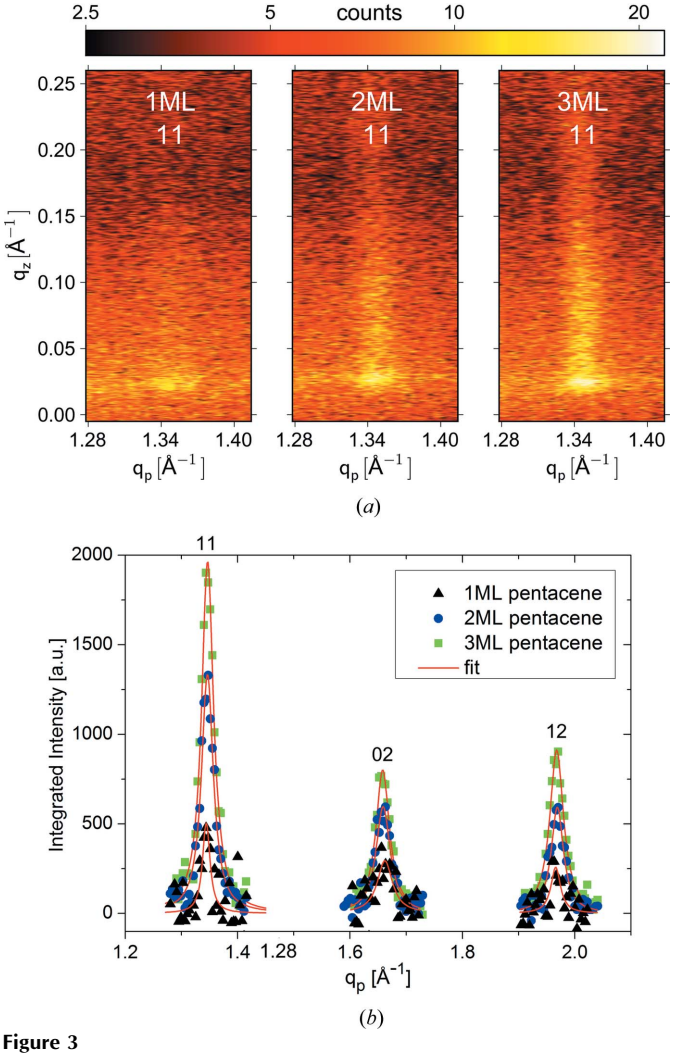

Figure 3
(*a*) Grazing-incidence reciprocal-space map of the 11 Bragg rod of nominally 1 ML, 2 ML and 3 ML pentacene on SiO_2. (*b*) Background-subtracted diffraction intensities of 1 ML, 2 ML and 3 ML pentacene integrated along the q_z direction (from 0 to 0.25 Å^{-1}) and plotted as a function of the in-plane scattering vector q_p (triangles, circles and squares). The first three Bragg rods are shown and fitted with Lorentzians (full lines).

Table 1
Two dimensional unit-cell parameters of 1 ML, 2 ML and 3 ML pentacene calculated from the fitted diffraction peak positions of Fig. 3(*b*).

The parameters obtained from our laboratory data are compared with parameters from previous studies of pentacene monolayer (Fritz *et al.*, 2004), sub-monolayer (SML) and multilayer (MML) (Ruiz *et al.*, 2004) samples (all from synchrotron measurements).

	a (Å)	*b* (Å)	γ (°)
1 ML (this work)	5.91 (6)	7.56 (3)	89.6 (5)
2 ML (this work)	5.92 (2)	7.58 (1)	90.0 (2)
3 ML (this work)	5.91 (1)	7.58 (1)	89.9 (2)
1 ML (Fritz *et al.*, 2004)	5.916	7.588	89.95
SML (Ruiz *et al.*, 2004)	5.90	7.62	90.0 (2)
MML (Ruiz *et al.*, 2004)	5.91	7.58	90.0 (2)

because of the presence of two polymorph structures of pentacene appearing at similar q_p positions (compare Fig. 2*a*). Nevertheless, the in-plane resolution is quite sufficient to characterize organic thin films, although caution is advised when performing crystal size determinations by peak breadth analysis. The resolution limit for grain size analysis is reached if the peak broadening due to the crystal grain size does not exceed the broadening due to the apparatus resolution by at least 50% (Smilgies, 2009). For the presented setup this leads to a maximum in-plane crystal size of 25 nm accessible to grain size determinations. Transverse shear force microscopy studies on pentacene monolayers vacuum deposited on SiO_2 report lateral crystalline domain sizes of 1–2 µm (Zhang *et al.*, 2008; Wu *et al.*, 2009); thus the observed peak broadening is purely caused by the in-plane resolution of the setup.

4.2. Pentacene mono- and multilayers

Pentacene films of nominally one-monolayer (1 ML; 1.3 nm), 2 ML (2.6 nm) and 3 ML (3.9 nm) thickness were prepared by vacuum deposition on thermally oxidized silicon wafers. The RSMs of the first Bragg rod of the 1 ML, 2 ML and 3 ML samples are shown in Fig. 3(*a*). A step size of $\Delta 2\theta_i = 0.05°$ was chosen using an integration time of 360 s per step. The rod-like shape of the diffraction features originates from the absence of a periodicity perpendicular to the substrate surface that is characteristic for monolayer films. As expected, for the 2 and 3 ML samples, the evolution of a three-dimensional structure is observed by the emergence of Bragg peaks at out-of-plane q_z values for the 02 and 12 Bragg rods (see supplementary figure[1]). However, the quality of these Bragg rod profiles, especially for 1 ML, is not sufficient to perform quantitative analyses of the profiles. Background-subtracted integral intensity diffraction profiles (integrated over a q_z range from 0 to 0.25 Å^{-1}) for the 1 ML, 2 ML and 3 ML samples are shown in Fig. 3(*b*) for the first three Bragg rods. Because the indexing of the first three rods (11, 02 and 12) is known from previous work (Fritz *et al.*, 2004), the two-dimensional unit-cell parameters can be calculated from the q_p positions of the rods (obtained by fitting the integrated diffraction profiles with Lorentzians). The resulting parameters are summarized in Table 1 and show perfect agreement with previous studies of pentacene mono- and multilayers carried out by Fritz *et al.* (2004) and Ruiz *et al.* (2004), both using synchrotron radiation.

5. Conclusion

In this work, we presented a novel laboratory setup for grazing-incidence X-ray diffraction and demonstrated that our experimental

[1] The supplementary material discussed in this paper is available from the IUCr electronic archives (Reference: RG5007). Services for accessing these data are described at the back of the journal.

approach provides an effective possibility to characterize organic thin films and monolayers in the laboratory on a reasonable timescale. Our results clearly demonstrate that high-quality GIXD studies can be performed with laboratory sources even in the monolayer range. We showed that the quantity of matter of one monolayer (6.52 electrons $Å^{-2}$) is sufficient to perform an in-plane X-ray diffraction study that allows the clear observation of Bragg rods.

This work was supported by the Austrian Science Fund (FWF):[S9708]. The authors thank W. Caliebe (DESY-HASYLAB, Hamburg, Germany) for experimental support.

References

Als-Nielsen, J., Jacquemain, D., Kjaer, K., Leveiller, F., Lahav, M. & Leiserowitz, L. (1994). *Phys. Rep.* **246**, 251–313.
Campbell, R. B., Robertson, J. M. & Trotter, J. (1962). *Acta Cryst.* **15**, 289–290.
Dosch, H. (1992). *Critical Phenomena at Surfaces and Interfaces: Evanescent X-ray and Neutron Scattering*, Springer Tracts in Modern Physics, Vol. 126. Berlin, Heidelberg: Springer.
Fritz, S. E., Martin, S. M., Frisbie, C. D., Ward, M. D. & Toney, M. F. (2004). *J. Am. Chem. Soc.* **126**, 4084–4085.
Kaganer, V. M., Möhwald, H. & Dutta, P. (1999). *Rev. Mod. Phys.* **71**, 779–819.
Khazins, D., Becker, B., Diawara, Y., Durst, R., He, B., Medved, S., Sedov, V. & Thorson, T. (2004). *IEEE Trans. Nucl. Sci.* **51**, 943–947.
Mannsfeld, S. C., Tang, M. L. & Bao, Z. (2011). *Adv. Mater.* **23**, 127–131.
Marra, W. C., Eisenberger, P. & Cho, A. Y. (1979). *J. Appl. Phys.* **50**, 6927–6933.
Mattheus, C. C., Dros, A. B., Baas, J., Meetsma, A., Boer, J. L. de & Palstra, T. T. M. (2001). *Acta Cryst.* C**57**, 939–941.
Moser, A. (2011). *PyGid: Software for the Analysis of Grazing-Incidence X-ray Diffraction Data*. Personal communication.
Moser, A., Werzer, O., Flesch, H., Koini, M., Smilgies, D., Nabok, D., Puschnig, P., Ambrosch-Draxl, C., Schiek, M., Rubahn, H. & Resel, R. (2009). *Eur. Phys. J. Spec. Top.* **167**, 59–65.
Nabok, D., Puschnig, P., Ambrosch-Draxl, C., Werzer, O., Resel, R. & Smilgies, D.-M. (2007). *Phys. Rev. B*, **76**, 235322.
Neuhold, A., Novák, J., Flesch, H.-G., Moser, A., Djuric, T., Grodd, L., Grigorian, S., Pietsch, U. & Resel, R. (2012). *Nucl. Instrum. Methods Phys. Res. Sect. B*, doi:10.1016/j.nimb.2011.07.105.
Novák, J., Oehzelt, M., Berkebile, S., Koini, M., Ules, T., Koller, G., Haber, T., Resel, R. & Ramsey, M. G. (2011). *Phys. Chem. Chem. Phys.* **13**, 14675–14684.
Resel, R., Oehzelt, M., Lengyel, O., Haber, T., Schulli, T., Thierry, A., Hlawacek, G., Teichert, C., Berkebile, S. & Koller, G. (2006). *Surf. Sci.* **600**, 4645–4649.
Ruiz, R., Mayer, A. C., Malliaras, G. G., Nickel, B., Scoles, G., Kazimirov, A., Kim, H., Headrick, R. L. & Islam, Z. (2004). *Appl. Phys. Lett.* **85**, 4926–4928.
Salzmann, I., Nabok, D., Oehzelt, M., Duhm, S., Moser, A., Heimel, G., Puschnig, P., Ambrosch-Draxl, C., Rabe, J. P. & Koch, N. (2011). *Cryst. Growth Des.* **11**, 600–606.
Schiefer, S., Huth, M., Dobrinevski, A. & Nickel, B. (2007). *J. Am. Chem. Soc.* **129**, 10316–10317.
Schuster, M. & Gobel, H. (1995). *J. Phys. D Appl. Phys.* **28**, A270–A275.
Smilgies, D.-M. (2009). *J. Appl. Cryst.* **42**, 1030–1034.
Tanner, B. K., Hase, T. P. A., Lafford, T. A. & Goorsky, M. S. (2004). *Powder Diffr.* **19**, 45–48.
Vineyard, G. H. (1982). *Phys. Rev. B*, **26**, 4146–4159.
Wu, Y., Toccoli, T., Zhang, J., Koch, N., Iacob, E., Pallaoro, A., Iannotta, S. & Rudolf, P. (2009). *Appl. Phys. A*, **95**, 21–27.
Yoshida, H., Inaba, K. & Sato, N. (2007). *Appl. Phys. Lett.* **90**, 181930.
Zhang, J., Rabe, J. P. & Koch, N. (2008). *Adv. Mater.* **20**, 3254–3257.